Algebraic Tuning Guidelines for Model Predictive Torque and Flux Control

Tobias Geyer, *Senior Member, IEEE*

Abstract—Finite control set model predictive torque and flux control uses a scalar weight in its cost function to determine the trade-off between the torque and flux magnitude tracking error terms. This weight strongly influences the current distortions. It will be shown that an optimal weight can be computed algebraically, which minimizes the current distortions. The resulting predictive torque and flux controller achieves current distortions per switching frequency that are very similar to those of a predictive current controller, provided that the corresponding weight on the switching effort is selected appropriately. To this end, a second analytical expression will be derived.

Index Terms—Model predictive control, finite control set, cost function, penalty weights, tuning, torque and flux control, current control, power converters, variable speed drives.

I. INTRODUCTION

Finite control set model predictive control (FCS-MPC) has become popular thanks to its versatility, and its algorithmic and computational simplicity [1]. In order to achieve the desired closed-loop performance characteristic, however, the weights in the cost function need to be selected carefully. This tuning process is usually performed on a trial-and-error basis [2] and is thus considered an unresolved issue [3].

An important member of the FCS-MPC family is predictive torque and flux control [4] for variable speed drives. By *directly* controlling the electromagnetic torque and the machine magnetization, a high degree of robustness to model parameter variations can be achieved [5]. The predicted torque and stator flux magnitude errors are penalized in the cost function. To determine the relative importance of these two terms, a penalty weight is introduced. The latter has a significant impact on the control performance, particularly on the harmonic current distortions, which tend to be worse than for predictive current control, as will be discussed in this paper.

To select the weights in FCS-MPC, the commonly followed approach is to run multiple closed-loop simulations for a range of weights and to then choose the combination of weights that minimizes a given performance criterium [6]–[9]. To simplify this process, it is advisable to normalize the controlled quantities [6], for example by adopting a per unit (pu) system. To speed up the selection process, optimization methods can be used to derive Pareto fronts, see [10].

On the other hand, an algebraic method was proposed in [11] for predictive torque and flux control when applied to two-level inverters; when alternating between active and zero vectors, analytical expressions for the weights can be derived

The author is with ABB Corporate Research, Baden-Dättwil, Switzerland; e-mail: t.geyer@ieee.org

that minimize the torque ripple. By ranking the magnitude of each cost function term and then taking the minimum of their average value, the weights can be avoided altogether [12]. In effect, this leads to a discrete cost function, but nevertheless requires the tuning of the relative importance of the flux magnitude with respect to the electromagnetic torque.

Alternatively, by adopting the notion of field orientation [13], the torque and machine magnetization can be controlled *indirectly* through orthogonal stator current components [14] using the notion of predictive current control. This concept was introduced in [15] and later refined in [16]–[18]. It is generally accepted that the two orthogonal current components should be equally penalized to minimize the current distortions, see also [19] and [20]. A mathematical justification is provided in Appendix A. To reduce the switching frequency, the predicted number of commutations should also be penalized in the cost function. The associated trade-off between current tracking and switching frequency is fundamental to power electronics and well understood, see for example [21]. Alas, the commutations are often not penalized in the literature.

This paper aims to improve the understanding of the weight selection process in predictive torque and flux control by answering two questions: First, what are the optimal weights on the torque and flux error terms that achieve minimal current distortions for a given switching frequency? It turns out that a simple analytical expression can be derived.

Second, motivated by the observation that predictive current control achieves lower current distortions than predictive torque and flux control, is it possible to tune the latter controller such that it becomes equivalent to the predictive current controller in terms of the current distortions per switching frequency? An analysis of the cost function level sets shows that this is, in general, impossible. An analytical expression for the weights can nevertheless be derived that makes both controllers perform in as similar a manner as possible.

In summary, this paper provides tuning guidelines for the two most commonly used predictive control methods. These tuning guidelines are simple algebraic equations. A preliminary version of this paper is available at [22].

For illustrative purposes, a medium-voltage (MV) drive system with a three-level neutral point clamped (NPC) inverter and an induction machine will be considered. To simplify the exposition, the neutral point potential will be assumed to be zero, and a pu system will be adopted to normalize all quantities. We will restrict the prediction horizon to one step, as this variant of FCS-MPC is the one that is most widely used.
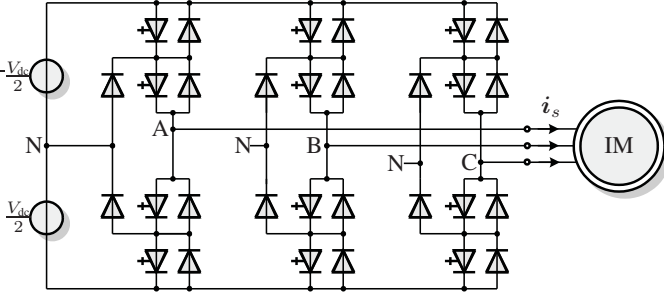
Fig. 1: NPC inverter with an induction motor and a fixed neutral point potential

For long-horizon FCS-MPC, the interested reader is referred to [23] and [24].

The paper is structured as follows. Sect. II summarizes the drive system case study and its mathematical model. Predictive torque and flux control is reviewed and its cost function is analyzed in Sect. III, whereas Sect. IV summarizes predictive current control. The main contribution of this paper, the procedure to select the optimal weights using algebraic equations, is provided in Sect. V. Sect. VI evaluates the performance of the two predictive controllers. Sect. VII provides a summary of the paper and conclusions. Appendix A shows that for predictive current control the common choice of equal weights on the two orthogonal current components minimizes the current distortions. Appendix B discusses the trade-off between current and torque distortions for predictive control.

II. DRIVE SYSTEM CASE STUDY

Consider an NPC voltage source inverter connected to an MV induction machine, as shown in Fig. 1. A $3.3\,\text{kV}$ and $50\,\text{Hz}$ squirrel-cage induction machine rated at $2\,\text{MVA}$ is used. The dc-link voltage is assumed to be constant at $V_{\text{dc}} = 5.2\,\text{kV}$, and the potential of the neutral point N is fixed to zero.

Throughout the paper, we will use normalized quantities. The pu system is established using the base quantities $V_B = \sqrt{2/3}V_{\text{rat}} = 2694\,\text{V}$, $I_B = \sqrt{2}I_{\text{rat}} = 503.5\,\text{A}$ and $f_B = f_{\text{rat}} = 50\,\text{Hz}$. We also normalize the time axis t, with one time unit corresponding to $1/(2\pi f_B)$ seconds. The rated

Voltage	3300 V
Current	356 A
Real power	1.587 MW
Apparent power	2.035 MVA
Stator frequency	50 Hz
Rotational speed	596 rpm

TABLE I: Rated values of the drive system

Stator resistance	$R_s = 0.0108$
Rotor resistance	$R_r = 0.0091$
Stator leakage reactance	$X_{ls} = 0.1493$
Rotor leakage reactance	$X_{lr} = 0.1104$
Main reactance	$X_m = 2.349$
Total leakage reactance	$X_\sigma = 0.2548$
dc-link voltage	$V_{\text{dc}} = 1.930$

TABLE II: Parameters of the drive system in the per unit system

values and the detailed parameters of the machine and inverter are summarized in Tables I and II, respectively.

A. Reference Frames

All variables $\boldsymbol{\xi}_{abc} = [\xi_a\ \xi_b\ \xi_c]^T$ in the three-phase (abc) system can be transformed to $\boldsymbol{\xi}_{dq} = [\xi_d\ \xi_q]^T$ in the orthogonal rotating dq reference frame through $\boldsymbol{\xi}_{dq} = \boldsymbol{K}(\varphi)\,\boldsymbol{\xi}_{abc}$ with

$$\boldsymbol{K}(\varphi) = \frac{2}{3}\begin{bmatrix} \cos(\varphi) & \cos(\varphi - \frac{2\pi}{3}) & \cos(\varphi + \frac{2\pi}{3}) \\ -\sin(\varphi) & -\sin(\varphi - \frac{2\pi}{3}) & -\sin(\varphi + \frac{2\pi}{3}) \end{bmatrix}.$$

In here, φ denotes the angle between the a-axis of the three-phase system and the d-axis of the reference frame, which is aligned with the rotor flux vector. The reference frame rotates with the angular speed $\omega_{\text{fr}} = \omega_s = \text{d}\varphi/\text{d}t$, where ω_s is the synchronous (or stator) angular frequency.

The stationary $\alpha\beta$ reference frame is obtained by setting φ and ω_{fr} to zero. The d- and q-axes are then referred to as α- and β-axes, respectively, and we write $\boldsymbol{\xi}_{\alpha\beta} = [\xi_\alpha\ \xi_\beta]^T = \boldsymbol{K}(0)\boldsymbol{\xi}_{abc}$.

B. Modeling based on the Rotor Flux Linkage

We model the induction machine in the stationary reference frame. A common choice is to write the dynamic machine equations in terms of the stator current vector $\boldsymbol{i}_{s,\alpha\beta}$ and the rotor flux linkage vector $\boldsymbol{\psi}_{r,\alpha\beta}$. Using these vectors as the state variables and treating the electrical angular speed of the rotor ω_r as a parameter, the continuous-time state-space model of the induction machine

$$\frac{\text{d}\boldsymbol{i}_{s,\alpha\beta}}{\text{d}t} = -\frac{1}{\tau_s}\boldsymbol{i}_{s,\alpha\beta} + \left(\frac{1}{\tau_r}\boldsymbol{I} - \omega_r\boldsymbol{Q}\right)\frac{X_m}{D}\boldsymbol{\psi}_{r,\alpha\beta} + \frac{X_r}{D}\boldsymbol{v}_{s,\alpha\beta} \tag{1a}$$

$$\frac{\text{d}\boldsymbol{\psi}_{r,\alpha\beta}}{\text{d}t} = \frac{X_m}{\tau_r}\boldsymbol{i}_{s,\alpha\beta} + \left(\omega_r\boldsymbol{Q} - \frac{1}{\tau_r}\boldsymbol{I}\right)\boldsymbol{\psi}_{r,\alpha\beta} \tag{1b}$$

can be obtained with the rotation matrix $\boldsymbol{Q} = \begin{bmatrix} 0 & -1 \\ 1 & 0 \end{bmatrix}$ and the two-dimensional identity matrix $\boldsymbol{I}$. The model parameters are the stator (rotor) resistance R_s (R_r), the stator (rotor) leakage reactance X_{ls} (X_{lr}) and the main reactance X_m. Furthermore, we define $X_s = X_{ls} + X_m$, $X_r = X_{lr} + X_m$ and $D = X_sX_r - X_m^2$. Note that all rotor quantities are referred to the stator circuit. The transient stator and rotor time constants are defined as

$$\tau_s = \frac{X_r D}{R_s X_r^2 + R_r X_m^2} \quad \text{and} \quad \tau_r = \frac{X_r}{R_r}, \tag{2}$$

respectively. For an excellent reference on electrical machines, the interested reader is referred to [25].

The stator voltage is given by

$$\boldsymbol{v}_{s,\alpha\beta} = \frac{1}{2}V_{\text{dc}}\boldsymbol{K}(0)\,\boldsymbol{u}, \tag{3}$$

where $\boldsymbol{u} = [u_a\ u_b\ u_c]^T$ is the three-phase switch position. The switch positions in the three phase legs are u_a, u_b, u_c, which are restricted to the set $\{-1, 0, 1\}$ for a three-level converter.
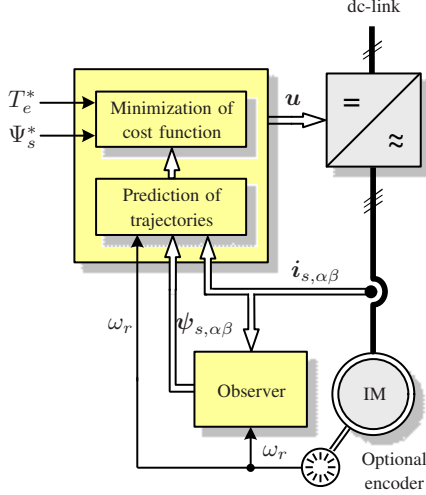
Fig. 2: Block diagram of the predictive torque and flux controller

The electromagnetic torque is given by

$$T_e = \frac{1}{\text{pf}} \frac{X_m}{X_r} \, \boldsymbol{\psi}_{r,\alpha\beta} \times \boldsymbol{i}_{s,\alpha\beta} = \frac{1}{\text{pf}} \frac{X_m}{X_r} \left(\psi_{r\alpha} i_{s\beta} - \psi_{r\beta} i_{s\alpha} \right), \quad (4)$$

where the operator $\times$ refers to the cross product. The power factor is given by $\text{pf} = P_{\text{rat}}/S_{\text{rat}}$, with P_{rat} and S_{rat} referring to the rated real and apparent power, respectively. Note that the per unit system is based on the apparent power, whereas the real power relates to the electromagnetic torque. The inverse of the power factor in (4) ensures that $T_e = 1 \, \text{pu}$ corresponds to rated torque.

C. Modeling based on the Stator Flux Linkage

Alternatively, by inserting the expression

$$\boldsymbol{\psi}_{r,\alpha\beta} = \frac{X_r}{X_m} \boldsymbol{\psi}_{s,\alpha\beta} - \frac{D}{X_m} \boldsymbol{i}_{s,\alpha\beta} \quad (5)$$

into (1), we obtain after several algebraic manipulations the state-space model

$$\frac{\mathrm{d}\boldsymbol{i}_{s,\alpha\beta}}{\mathrm{d}t} = \left(\omega_r \boldsymbol{Q} - \frac{R_s X_r + R_r X_s}{D} \boldsymbol{I} \right) \boldsymbol{i}_{s,\alpha\beta} +$$
$$+ \left(\frac{R_r}{D} \boldsymbol{I} - \omega_r \boldsymbol{Q} \frac{X_r}{D} \right) \boldsymbol{\psi}_{s,\alpha\beta} + \frac{X_r}{D} \boldsymbol{v}_{s,\alpha\beta} \quad (6a)$$

$$\frac{\mathrm{d}\boldsymbol{\psi}_{s,\alpha\beta}}{\mathrm{d}t} = -R_s \boldsymbol{i}_{s,\alpha\beta} + \boldsymbol{v}_{s,\alpha\beta} \,. \quad (6b)$$

This model uses the stator current vector $\boldsymbol{i}_{s,\alpha\beta}$ and the *stator flux linkage* vector $\boldsymbol{\psi}_{s,\alpha\beta}$ as state variables.

The torque equation (4) simplifies with the help of (5) to

$$T_e = \frac{1}{\text{pf}} \boldsymbol{\psi}_{s,\alpha\beta} \times \boldsymbol{i}_{s,\alpha\beta} = \frac{1}{\text{pf}} (\psi_{s\alpha} i_{s\beta} - \psi_{s\beta} i_{s\alpha}) \,. \quad (7)$$

Last, we define the magnitude of the stator flux vector as

$$\Psi_s = ||\boldsymbol{\psi}_{s,\alpha\beta}||_2 = \sqrt{\psi_{s\alpha}^2 + \psi_{s\beta}^2} \,. \quad (8)$$

III. Predictive Torque and Flux Control

The block diagram of the predictive torque and flux controller is shown in Fig. 2. The controller tracks the references of the electromagnetic torque T_e^* and stator flux magnitude Ψ_s^* by manipulating the three-phase switch position $\boldsymbol{u} \in \{-1, 0, 1\}^3$ [9]. At the same time, the switching frequency is minimized.

The controller is based on the stator current measurement and the stator flux estimate, which is estimated based on the measured stator current and the stator voltage. The latter is typically not measured, but it is rather reconstructed using the dc-link voltage and the three-phase switch position. The torque reference T_e^* is usually adjusted by an outer speed control loop. The magnetization of the machine is typically controlled via the stator rather than the rotor flux magnitude by setting the stator flux magnitude to $\Psi_s^* = 1 \, \text{pu}$, see, for example, [1]–[6], [8], [9]. The controller structure is thus simple, only requiring a speed controller and a stator flux observer. In particular, rotor flux information is not required.

A. Controller Model

The controller model predicts the electromagnetic torque and the magnitude of the stator flux vector at the next discrete time step $k + 1$ as a function of the to-be-determined switch position $\boldsymbol{u}(k)$ at the current time step k. These predictions are based on the machine model (6) in the stationary orthogonal $\alpha\beta$ reference frame. Let T_s denote the sampling interval. Integrating (6) from $t = kT_s$ to $t = (k+1)T_s$ with the forward Euler method and inserting (3) into it leads to the discrete-time representation

$$\boldsymbol{i}_{s,\alpha\beta}(k + 1) = \boldsymbol{A}_1 \boldsymbol{i}_{s,\alpha\beta}(k) + \boldsymbol{B}_1 \boldsymbol{\psi}_{s,\alpha\beta}(k) + \boldsymbol{B}_2 \boldsymbol{u}(k) \quad (9a)$$

$$\boldsymbol{\psi}_{s,\alpha\beta}(k + 1) = \boldsymbol{\psi}_{s,\alpha\beta}(k) + \boldsymbol{B}_3 \boldsymbol{i}_{s,\alpha\beta}(k) + \boldsymbol{B}_4 \boldsymbol{u}(k) \,. \quad (9b)$$

The system and input matrices are defined as

$$\boldsymbol{A}_1 = \boldsymbol{I} + \left(\omega_r \boldsymbol{Q} - \frac{R_s X_r + R_r X_s}{D} \boldsymbol{I} \right) T_s,$$

$$\boldsymbol{B}_1 = \left(\frac{R_r}{D} \boldsymbol{I} - \omega_r \boldsymbol{Q} \frac{X_r}{D} \right) T_s, \quad \boldsymbol{B}_2 = \frac{X_r}{D} \frac{V_{\text{dc}}}{2} \boldsymbol{K}(0) \, T_s,$$

$$\boldsymbol{B}_3 = -R_s \boldsymbol{I} \, T_s, \quad \boldsymbol{B}_4 = \frac{V_{\text{dc}}}{2} \boldsymbol{K}(0) \, T_s \,.$$

B. Optimization Problem

Over a one-step horizon, we define the cost function

$$J_1 = J_T + J_\Psi + J_{uT} \quad (10)$$

with the terms

$$J_T = \lambda_T \big(T_e^*(k + 1) - T_e(k + 1) \big)^2, \quad (11a)$$

$$J_\Psi = (1 - \lambda_T) \big(\Psi_s^*(k + 1) - \Psi_s(k + 1) \big)^2, \quad (11b)$$

$$J_{uT} = \lambda_{uT} ||\Delta \boldsymbol{u}(k)||_1 \,. \quad (11c)$$

The first term penalizes the predicted deviation of the electromagnetic torque from its reference at time step $k + 1$. Accordingly, the second term penalizes the predicted deviation of the stator flux magnitude from its reference. Both

(a) Torque error term J_T

(b) Flux magnitude error term J_Ψ

(c) Sum $J_T + J_\Psi$ of the torque error and stator flux magnitude error terms
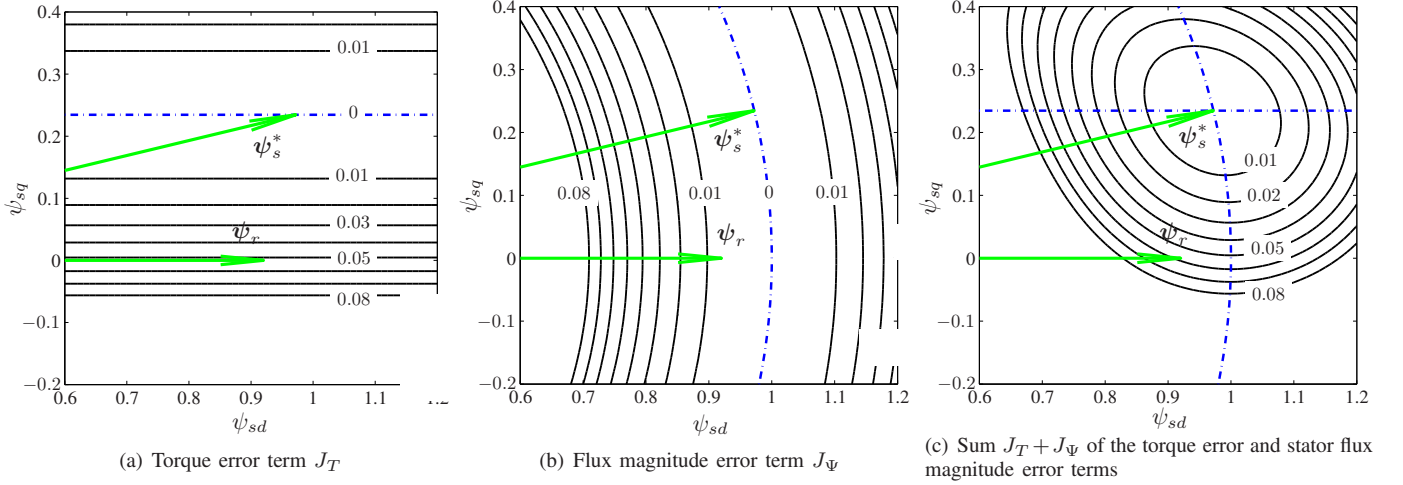
Fig. 3: Contour maps of the cost function terms of the predictive torque and flux controller in a plane spanned by the d- and q-components of the stator flux vector. The reference stator flux and the rotor flux vectors are shown as arrows

terms are penalized quadratically. The third term penalizes the switching effort at time step k, using the non-negative scalar weight λ_{uT} and the change in the switch position $\Delta \boldsymbol{u}(k) = \boldsymbol{u}(k) - \boldsymbol{u}(k-1)$.

The weight λ_T is introduced to discount the torque ripple and to prioritize the flux magnitude ripple, without changing the cost ratio between these two terms and the switching effort. In general, in order to obtain low current distortions, the stator flux ripple needs to be much smaller than the torque ripple. This can be achieved, for example, by setting λ_T to 0.1. The impact of λ_T on the current distortion will be analyzed in Sect. VI. To ensure that J_1 is non-negative, the weight λ_T is bounded between zero and one.

The optimization problem of the predictive torque and flux controller with reference tracking and a prediction horizon of one step can now be stated as

$$\boldsymbol{u}_{\text{opt}}(k) = \arg \underset{\boldsymbol{u}(k)}{\text{minimize}} \; J_T + J_\Psi + J_{uT} \qquad (12a)$$

$$\text{subject to (9)} \qquad (12b)$$

$$T_e(k+1) = \frac{1}{\text{pf}} \, \boldsymbol{\psi}_{s,\alpha\beta}(k+1) \times \boldsymbol{i}_{s,\alpha\beta}(k+1) \qquad (12c)$$

$$\Psi_s(k+1) = ||\boldsymbol{\psi}_{s,\alpha\beta}(k+1)||_2 \qquad (12d)$$

$$\boldsymbol{u}(k) \in \{-1, 0, 1\}^3, \; ||\Delta \boldsymbol{u}(k)||_\infty \leq 1 \,. \qquad (12e)$$

Note that $||\Delta \boldsymbol{u}||_\infty$ denotes the infinity-norm of the vector $\Delta \boldsymbol{u}$, which is defined as the component of $\Delta \boldsymbol{u}$ with the largest absolute value, i.e. $||\Delta \boldsymbol{u}||_\infty = \max(|\Delta u_a|, |\Delta u_b|, |\Delta u_c|)$.

One of the advantages of this control problem formulation is that the torque and flux references are constant during steady-state operation. Hence we may assume that $T_e^*(k+1) = T_e^*(k)$ and $\Psi_s^*(k+1) = \Psi_s^*(k)$.

C. Control Algorithm

The optimization problem (12) is typically solved by enumerating all switch positions and computing the cost for each.

The switch position at time step k with the minimum cost, $\boldsymbol{u}_{\text{opt}}(k)$, is by definition the optimal one, see for example [1] and [26].

D. Analysis

To analyse the predictive torque and flux controller, it is convenient to adopt the dq reference frame rotating in synchronism with the rotor flux. The latter is not required by the controller, but eases the analysis. Furthermore, to improve the readability, we drop in this section the time dependence of the variables.

The torque equation (4) and the flux expression (5) also hold in the dq reference frame, for which we replace the subindices $\alpha\beta$ by dq. Inserting (5) into (4) leads to the electromagnetic torque in the dq reference frame

$$T_e = \frac{1}{\text{pf}} \frac{X_m}{D} \, \boldsymbol{\psi}_{r,dq} \times \boldsymbol{\psi}_{s,dq} = \frac{1}{\text{pf}} \frac{X_m}{D} \left(\psi_{rd} \psi_{sq} - \psi_{rq} \psi_{sd} \right) . \qquad (13)$$

By aligning the rotor flux vector with the d-axis, (13) simplifies to

$$T_e = \frac{1}{\text{pf}} \frac{X_m}{D} \psi_{rd} \psi_{sq} \,. \qquad (14)$$

With this, and noting that

$$\Psi_s = ||\boldsymbol{\psi}_{s,dq}||_2 = \sqrt{\psi_{sd}^2 + \psi_{sq}^2} \,, \qquad (15)$$

the tracking error terms of the cost function can be expressed in terms of the d- and q-components of the stator flux vector. We rewrite (11a) and (11b) as

$$J_T = \lambda_T \left(\frac{1}{\text{pf}} \frac{X_m}{D} \psi_{rd} \right)^2 \left(\psi_{sq}^* - \psi_{sq} \right)^2 \text{ and} \qquad (16a)$$

$$J_\Psi = (1 - \lambda_T) \left(||\boldsymbol{\psi}_{s,dq}^*||_2 - ||\boldsymbol{\psi}_{s,dq}||_2 \right)^2 . \qquad (16b)$$
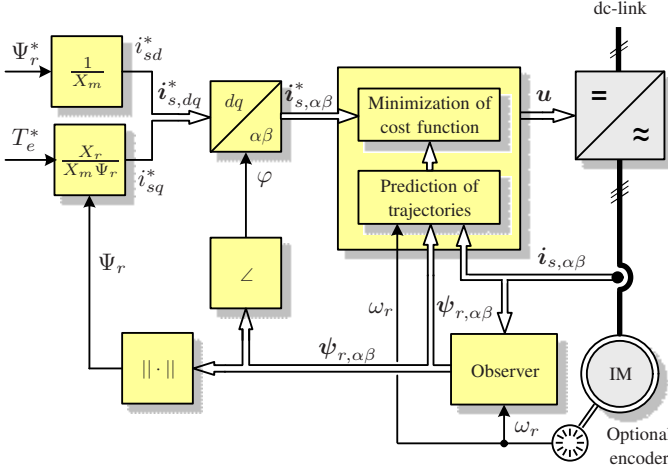
Fig. 4: Block diagram of the predictive current controller

The reference of the stator flux vector is obtained from (14) and (15) as

$$\psi_{sq}^* = \text{pf}\frac{D}{X_m}\frac{T_e^*}{\psi_{rd}} \tag{17a}$$

$$\psi_{sd}^* = \sqrt{(\Psi_s^*)^2 - (\psi_{sq}^*)^2}\,. \tag{17b}$$

Note that ψ_{rd} is equal to the magnitude of the rotor flux vector.

To visualize the two cost function terms in (16), consider the MV induction machine operating at nominal speed and rated torque. A geometrical representation of the torque error term J_T is provided in Fig. 3(a). The rotor flux vector is aligned with the d-axis. The reference of the stator flux vector corresponds to nominal torque and a fully magnetized machine. The contour lines of the torque error term J_T with the weight $\lambda_T = 0.052$ are shown as solid lines for the contour values $0.01, 0.02, \dots, 0.08$. The dash-dotted line refers to $J_T = 0$. Owing to (14), the contour lines are straight lines that are parallel to the rotor flux vector.

Accordingly, the cost function term J_Ψ of the stator flux magnitude error is illustrated in Fig. 3(b). The contour lines of J_Ψ are depicted again for the values $0.01, 0.02, \dots, 0.08$. These contour lines form concentric circles that are centered on the origin of the dq reference frame. The dash-dotted line refers to $J_\Psi = 0$. Adding the two cost functions terms to $J_T + J_\Psi$ leads to the contour map shown in Fig. 3(c).

IV. Predictive Current Control

The current control problem is typically formulated in the stationary $\alpha\beta$ reference frame. The objective of the current controller is to manipulate the three-phase switch position $\boldsymbol{u}$ such that the stator current $\boldsymbol{i}_{s,\alpha\beta}$ closely tracks its reference $\boldsymbol{i}_{s,\alpha\beta}^*$, while minimizing the switching frequency.

The block diagram of the predictive current controller is shown in Fig. 4. The controller predicts the stator current at the next time step for all admissible switch positions. For the prediction, the measured stator current is required, along with the rotor flux vector, which is constructed by an observer.

Outer control loops are required, which are formulated in the rotating dq reference frame with the angular position φ of the rotor flux vector. These control loops provide the stator current reference $\boldsymbol{i}_{s,dq}^*$ in dq, which serves—after being translated into the stationary $\alpha\beta$ coordinate system—as the reference $\boldsymbol{i}_{s,\alpha\beta}^*$ to the predictive current controller. The feedforward terms shown in Fig. 4 for the magnetization and torque controllers are typically augmented by PI control loops. As the dynamics of the outer loops are slower than those of the inner loop—typically by an order of magnitude—we neglect them in the following to simplify the exposition.

A. Controller Model

To predict future stator currents as a function of the three-phase switch position $\boldsymbol{u}$, we adopt the machine model (1) based on the rotor flux linkage. The forward Euler discretization method directly leads to the discrete-time representation

$$\boldsymbol{i}_{s,\alpha\beta}(k+1) = \boldsymbol{A}_2\boldsymbol{i}_{s,\alpha\beta}(k) + \boldsymbol{B}_5\boldsymbol{\psi}_{r,\alpha\beta}(k) + \boldsymbol{B}_6\boldsymbol{u}(k) \tag{18}$$

with the system and input matrices

$$\boldsymbol{A}_2 = \boldsymbol{I}(1 - \frac{1}{\tau_s}T_s),\ \ \boldsymbol{B}_5 = \left(\frac{1}{\tau_r}\boldsymbol{I} - \omega_r\boldsymbol{Q}\right)\frac{X_m}{D}T_s,$$

$$\boldsymbol{B}_6 = \frac{X_r}{D}\frac{V_{\text{dc}}}{2}\boldsymbol{K}(0)\,T_s\,.$$

Equation (18) allows one to predict the stator current at the next time step $k+1$. The rotor flux dynamic is not required, because we adopted a one-step prediction horizon and the forward Euler discretization method.

B. Optimization Problem

We define the cost function

$$J_2 = J_I + J_{uI} \tag{19}$$

with the stator current term J_I and the penalty on switching J_{uI}:

$$J_I = ||\boldsymbol{i}_{s,\alpha\beta}^*(k+1) - \boldsymbol{i}_{s,\alpha\beta}(k+1)||_2^2, \tag{20a}$$

$$J_{uI} = \lambda_{uI}||\Delta\boldsymbol{u}(k)||_1\,. \tag{20b}$$

Note that $||\boldsymbol{\xi}_{\alpha\beta}||_2^2 = \xi_\alpha^2 + \xi_\beta^2$ and $\lambda_{uI} \geq 0$. As shown in Appendix A, the term J_I approximates the total demand distortion (TDD) of the stator current, albeit very coarsely.

The optimization problem underlying one-step predictive current control with reference tracking follows as

$$\boldsymbol{u}_{\text{opt}}(k) = \arg \underset{\boldsymbol{u}(k)}{\text{minimize}}\ J_I + J_{uI} \tag{21a}$$

$$\text{subject to }(18) \tag{21b}$$

$$\boldsymbol{u}(k) \in \{-1, 0, 1\}^3,\ ||\Delta\boldsymbol{u}(k)||_\infty \leq 1\,. \tag{21c}$$

C. Analysis

We compare the contour plots of the predictive torque and flux controller with those of the predictive current controller. As previously, we drop the time dependence of the variables and perform the analysis in the rotating dq reference frame. As
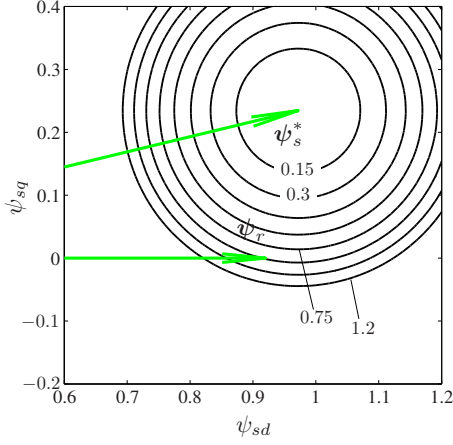
Fig. 5: Contour map of the current error term J_I of the predictive current controller

(a) Torque reference $T_e^* = 0.1\,\mathrm{pu}$

the transformation from the stationary to the rotating reference frame is amplitude-invariant, we can rewrite (20a) as

$$J_I = ||\boldsymbol{i}_{s,dq}^* - \boldsymbol{i}_{s,dq}||_2^2 . \tag{22}$$

We can express the stator current as a linear combination of the stator and rotor flux vectors using

$$\boldsymbol{i}_{s,dq} = \frac{1}{D}(X_r \boldsymbol{\psi}_{s,dq} - X_m \boldsymbol{\psi}_{r,dq}) , \tag{23}$$

see also (5). This allows us to rewrite the current error term (22) in terms of the stator flux:

$$J_I = \left(\frac{X_r}{D}\right)^2 ||\boldsymbol{\psi}_{s,dq}^* - \boldsymbol{\psi}_{s,dq}||_2^2 . \tag{24}$$

The contour lines of the current error term are shown in Fig. 5 as concentric circles around the stator flux reference. The contour lines are plotted for the values $0.15, 0.3, \ldots, 1.2$. Compared to the contour values used for the torque controller, these values are multiplied by a factor of 15.

V. TUNING GUIDELINES

When comparing the tracking error terms of the torque and flux controller (16) with that of the current controller (24), it is obvious that the cost functions of the two controllers are not equivalent. This observation is illustrated in Figs. 3(c) and 5 by the different shapes of the contour lines. Nevertheless, by appropriately tuning the weights in the cost functions, a large degree of similarity between the two controllers can be achieved. Specifically, as shown in the following, λ_T can be chosen such that the contour lines of the torque controller approximate circles, particularly when the torque is close to zero.

To simplify the exposition in the following derivation, we set the torque reference to zero. Consider the stator flux vector

$$\boldsymbol{\psi}_{s,dq} = \boldsymbol{\psi}_{s,dq}^* + \begin{bmatrix} \psi_{\mathrm{err}} \\ 0 \end{bmatrix} \tag{25}$$

with the flux error ψ_{err} in the d-axis. Note that $\psi_{sq}^* = 0$ because of our assumption that the torque reference is zero. According
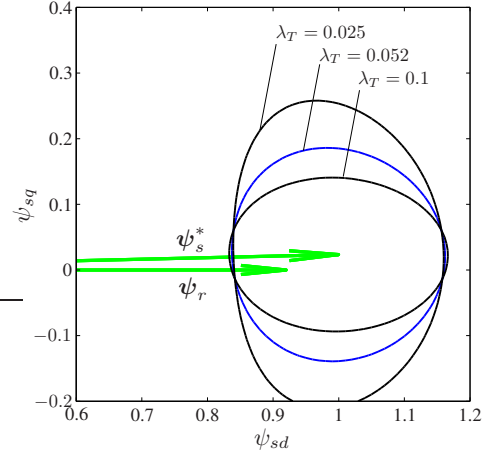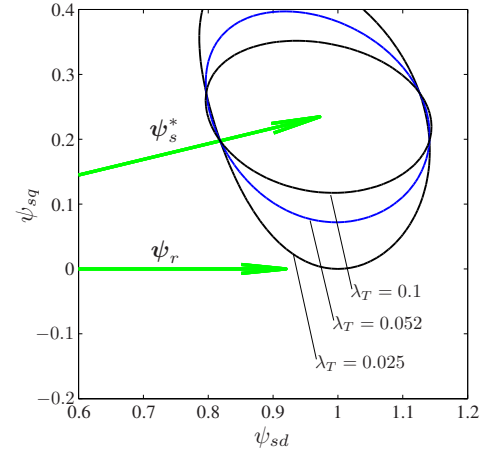
(b) Torque reference $T_e^* = 1\,\mathrm{pu}$

Fig. 6: Contour lines for the tracking error term $J_T + J_\Psi = 0.025$ of the predictive torque and flux controller for three different weighting factors λ_T

to (16), the cost of the tracking error terms is

$$J_T + J_\Psi = (1 - \lambda_T)\psi_{\mathrm{err}}^2 . \tag{26}$$

Similarly, for a stator flux vector with the flux error ψ_{err} in the q-axis, the cost is

$$J_T + J_\Psi = \lambda_T \left(\frac{1}{\mathrm{pf}}\frac{X_m}{D}\psi_{rd}\right)^2 \psi_{\mathrm{err}}^2 , \tag{27}$$

where we have neglected the minor contribution of J_Ψ. To achieve circular contour lines, both costs are required to be equal, which leads to

$$\lambda_T = \frac{(\mathrm{pf}\,D)^2}{(\mathrm{pf}\,D)^2 + (X_m \psi_{rd})^2} . \tag{28}$$

For the parameters of the considered drive system case study, we obtain $\lambda_T = 0.052$.

The validity of this choice is confirmed by Fig. 6(a), which depicts for three different λ_T the contour lines with the same cost $J_T + J_\Psi = 0.025$. When the torque reference is close to zero, $\lambda_T = 0.052$ leads to an effectively circular contour

TABLE III: Comparison of the predictive torque and flux controller with the predictive current controller in terms of the current TDD I_{TDD} and torque TDD T_{TDD}. The switching penalties are chosen such that a switching frequency of approximately $f_{\text{sw}} = 220\,\text{Hz}$ results

Torque reference (pu)	Control scheme	Controller settings	I_{TDD} (%)	T_{TDD} (%)	f_{sw} (Hz)
$T_e^* = 0$	Torque and flux	$\lambda_T = 0.052$, $\lambda_{uT} = 0.198 \cdot 10^{-3}$	6.45	5.76	219
$T_e^* = 0$	Current	$\lambda_{uI} = 3 \cdot 10^{-3}$	6.38	5.57	220
$T_e^* = 1$	Torque and flux	$\lambda_T = 0.052$, $\lambda_{uT} = 0.198 \cdot 10^{-3}$	7.74	5.84	221
$T_e^* = 1$	Current	$\lambda_{uI} = 3 \cdot 10^{-3}$	6.69	5.51	222

line. Variations in λ_T mostly affect the shape of the contour lines in the q-axis, which relates to the torque. Reducing λ_T, and hence the penalty on the torque error, widens the contour lines along the torque axis and increases the torque ripple. Conversely, when increasing λ_T and prioritizing the torque error, the torque ripple is reduced. In both cases, contour lines of elliptical shapes result. Note that variations of λ_T around 0.052 have only a minor effect on the contour lines along the d-axis, which relates to the stator flux magnitude and determines its ripple.

Increasing the torque reference from zero to one distorts the contour lines along the circular reference of the stator flux magnitude, as can be seen in Fig. 6(b). In particular, the circular shape of the contour line for $\lambda_T = 0.052$ becomes somewhat compromised. Nevertheless, as will be shown in the next section, the two predictive control schemes provide similar performance results at all torque setpoints, provided that λ_T and the penalties on switching are appropriately chosen.

Tuning of the latter is required, because the diameters of the (almost circular) reference tracking contour lines of the two control schemes differ; this can be seen when comparing Fig. 3(c) with Fig. 5. More specifically, errors in the stator flux vector are penalized more heavily for the current controller than for the torque controller. This implies that the switching penalty needs to be increased accordingly for the current controller to achieve the same switching frequency as the torque controller.

In the end, the *ratio* between the cost values of the tracking error and the switching penalty terms determines the controller response. To achieve a similar closed-loop behavior for the two predictive controllers, these ratios should be the same. We thus set

$$\frac{J_T + J_\Psi}{\lambda_{uT}||\Delta \boldsymbol{u}(k)||_1} = \frac{J_I}{\lambda_{uI}||\Delta \boldsymbol{u}(k)||_1} . \tag{29}$$

Consider again a zero torque reference, a stator flux error ψ_{err} in the d-axis and zero flux error in the q-axis as in (25). With (26) and (24), the expression (29) can be simplified to

$$\frac{(1 - \lambda_T)\psi_{\text{err}}^2}{\lambda_{uT}} = \left(\frac{X_r}{D}\right)^2 \frac{\psi_{\text{err}}^2}{\lambda_{uI}} . \tag{30}$$

This leads to

$$\lambda_{uI} = \left(\frac{X_r}{D}\right)^2 \frac{\lambda_{uT}}{1 - \lambda_T} . \tag{31}$$

We conclude that both control schemes issue very similar switching commands when their penalties are selected according to the following rules:

- For the torque controller, set λ_T according to (28). The second degree of freedom, the penalty on switching λ_{uT}, is selected such that the desired switching frequency is achieved.
- For the current controller, set its penalty on switching λ_{uI} according to (31).

These tuning guidelines depend on the rotor flux amplitude, see (28), and several machine parameters: the power factor pf, the stator and rotor leakage reactances X_{ls} and X_{lr}, and the main reactance X_m. The latter three parameters form D and X_r, see also Sect. II-B. It is clear that the guidelines hold independently of the speed ω_r and torque T_e.

When applying these tuning guidelines, the two predictive control schemes are expected to yield similar current and torque distortions for a given switching frequency. This statement will be substantiated in the next section through closed-loop simulations.

VI. PERFORMANCE EVALUATION

For the performance evaluation of the predictive controllers, consider again the MV drive system case study of Sect. II. For the predictive torque and flux controller, unless otherwise mentioned, we choose the penalty $\lambda_T = 0.052$ according to (28). This choice ensures almost circular contour lines for the torque and flux error term. The resulting reference tracking error term in the cost function of the torque and flux controller is as similar as possible to that of the current controller. The switching penalty is set to $\lambda_{uT} = 0.198 \cdot 10^{-3}$ to achieve a switching frequency of around 250 Hz. The sampling interval is set to $T_s = 25\,\mu\text{s}$.

A. Operation at Nominal Speed

In the following, we consider operation at nominal speed. At rated torque, the predictive torque and flux controller yields a current TDD of 7.74%, a torque TDD of 5.84% and a device switching frequency of 221 Hz. The corresponding stator currents, electromagnetic torque and switch positions are shown in Fig. 7 over one fundamental period.

As shown in Table III, the distortions and switching frequencies are similar to those obtained by the predictive current controller with the switching penalty $\lambda_{uI} = 3 \cdot 10^{-3}$. The latter closely matches the design guideline (31), i.e. $\lambda_{uI} = 16.25\lambda_{uT}$. In particular, the current controller achieves the same switching frequency as the torque and flux controller.

At zero torque, both controllers yield effectively the same current and torque TDDs, see Table III, whereas at rated torque the current TDD deteriorates by 16% when using the torque and flux instead of the current controller. This worsening is

(a) Three-phase stator current $\boldsymbol{i}_{s,abc}$ (pu)

(b) Electromagnetic torque T_e (pu)

(c) Three-phase switch position $\boldsymbol{u}$
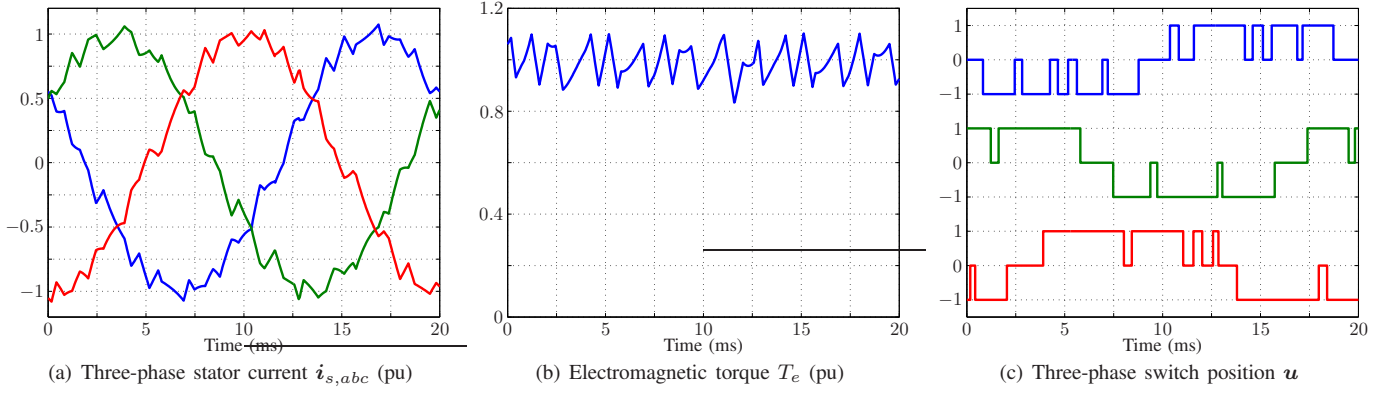
Fig. 7: Predictive torque and flux control during steady-state operation for $\lambda_T = 0.052$ and $\lambda_{uT} = 0.198 \cdot 10^{-3}$, with $I_{\mathrm{TDD}} = 7.74\%$ and $f_{\mathrm{sw}} = 221\,\mathrm{Hz}$

(a) Three-phase stator current $\boldsymbol{i}_{s,abc}$ (pu)

(b) Electromagnetic torque T_e (pu)

(c) Three-phase switch position $\boldsymbol{u}$
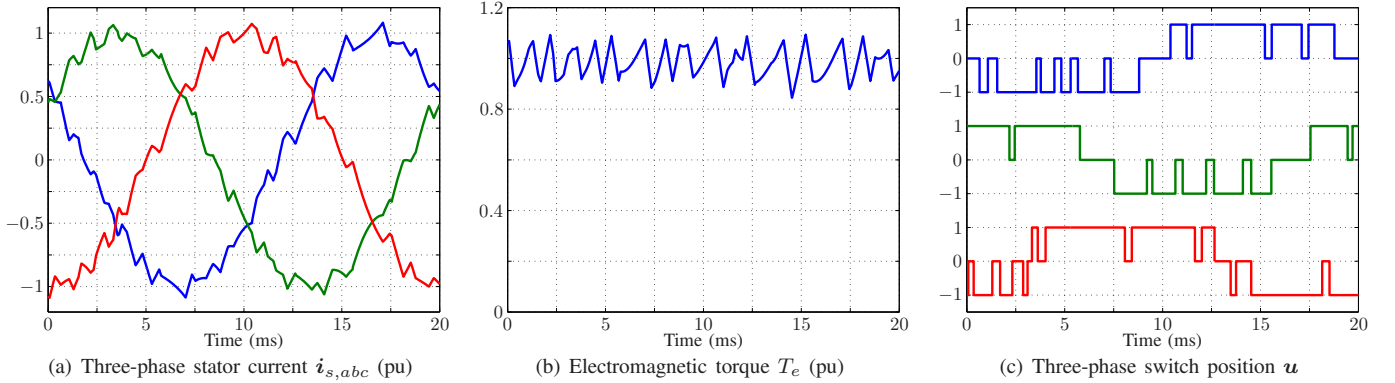
Fig. 8: Predictive current control during steady-state operation for $\lambda_{uI} = 3 \cdot 10^{-3}$, with $I_{\mathrm{TDD}} = 6.69\%$ and $f_{\mathrm{sw}} = 222\,\mathrm{Hz}$

due to the slightly non-circular shape of the contour lines for the stator flux error, which results in non-circular contour lines for the stator current error. The latter defines the current ripple and the current TDD. Nevertheless, at rated torque, the stator current ripple, torque ripple and the switching pattern are similar to those of the current controller. This can be seen when comparing Figs. 7 and 8. The instantaneous values are, however, different at rated torque, owing to the slightly different cost functions. Note that at zero torque, also the instantaneous values are very similar.

Similarly, when applying step changes in the torque reference, both controllers exhibit effectively the same transient behavior, provided that the above stated tuning guidelines are followed.

B. Trade-Off between Distortions and Switching Frequency at Nominal Speed and Rated Torque

Consider the torque and flux controller when operating at nominal speed and rated torque. To determine the trade-off between distortions and switching frequency, the penalty on switching, λ_{uT}, was varied between $0.02 \cdot 10^{-3}$ and $4 \cdot 10^{-3}$. Four different torque weights λ_T were considered; for each one about 500 simulations were run, leading to the approximately hyperbolic trade-off curves in Fig. 9.

Fig. 9(a) shows the influence λ_T has on the current TDD.

The value of $\lambda_T = 0.052$ clearly minimizes the current TDD, confirming the cost function analysis provided in Sect. V. For the torque TDD, however, the relatively small penalty of $\lambda_T = 0.052$ leads to relatively large torque distortions, as shown in Fig. 9(b). Increasing the penalty fivefold to 0.25, for example, halves the torque TDD throughout the considered switching frequency range from $50\,\mathrm{Hz}$ to $1.2\,\mathrm{kHz}$. This reduction in the torque TDD, however, comes at the price of pronounced current distortions, see Fig. 9(a) and Appendix B for an explanation. Nevertheless, for some applications, very low torque TDDs might be beneficial. The weight λ_T endows the torque controller with a degree of freedom to facilitate this.

Fig. 10 compares the current controller with the torque and flux controller; the latter uses the weight $\lambda_T = 0.052$ to minimize the current TDD. The penalties on switching, λ_{uI} and λ_{uT}, are varied for the two controllers to investigate operation at different switching frequencies. To ensure a strong similarity between the two control methods, the ratio $\lambda_{uI} = 16.25\lambda_{uT}$ is adopted, in accordance with the design guideline (31).

The resulting current and torque TDDs versus the switching frequency in Fig. 10 confirm the strong similarity between the two control schemes. For switching frequencies in excess of $250\,\mathrm{Hz}$, both schemes yield almost identical current and torque TDDs for a given switching frequency, with the current controller slightly outperforming the torque and flux
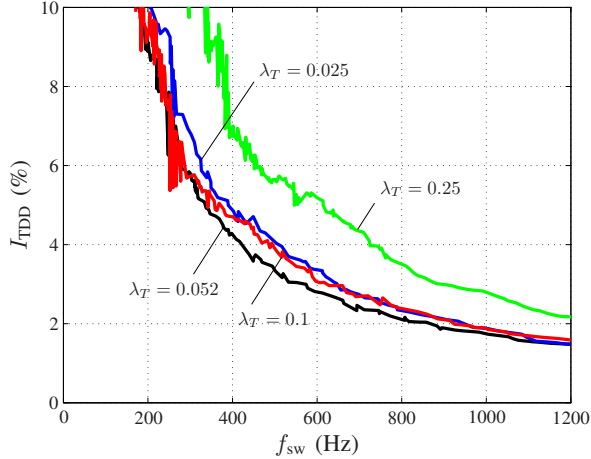
(a) Current TDD versus switching frequency
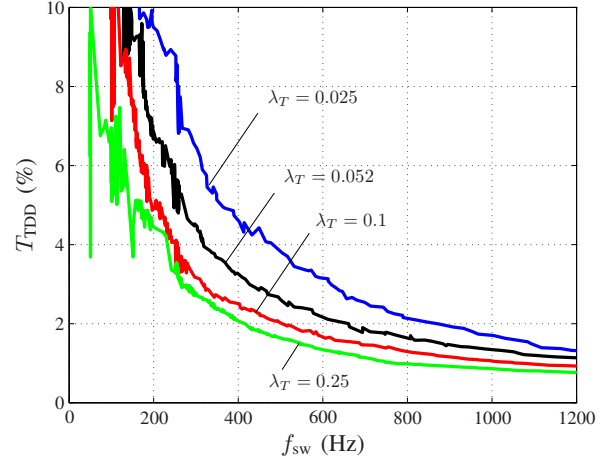
(b) Torque TDD versus switching frequency

Fig. 9: Predictive torque and flux control with different torque weights λ_T when operating at nominal speed and rated torque
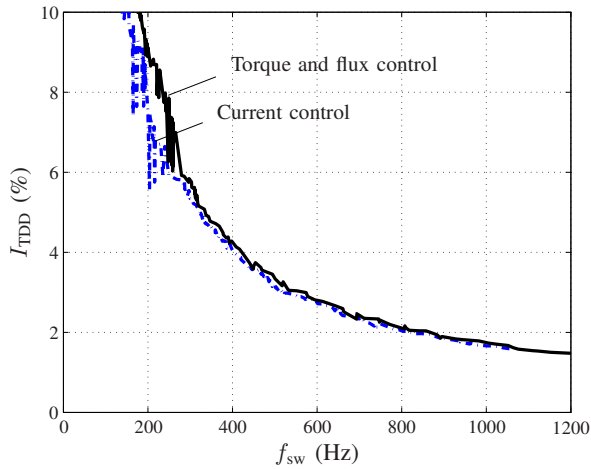
(a) Current TDD versus switching frequency
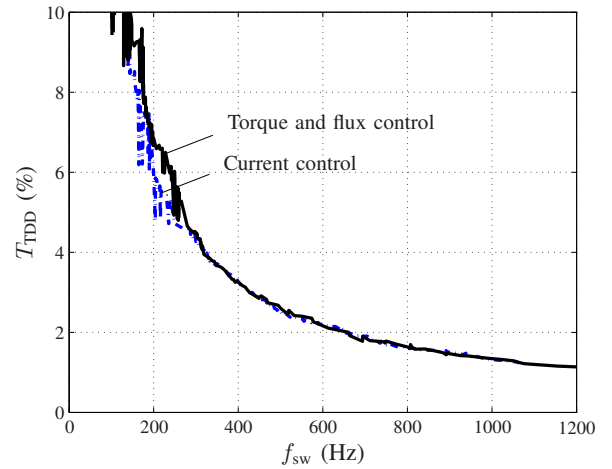
(b) Torque TDD versus switching frequency

Fig. 10: Predictive torque and flux control with $\lambda_T = 0.052$ is compared with predictive current control when operating at nominal speed and rated torque

controller. This small difference becomes more pronounced at low switching frequencies.

When the two predictive controllers operate at low switching frequencies, the switching frequency tends to lock into integer multiples of the fundamental frequency, such as $50, 100, \ldots, 250$ Hz, despite significant variations in the switching penalty. This phenomenon can be seen in Figs. 9 and 10. It implies a certain degree of periodicity in the switching actions and a somewhat discrete current spectrum. This feature is more pronounced in the case of long prediction horizons, as discussed and analyzed in [24].

C. Operation at Multiple Speed Operating Points

Last, we consider operation at various speed operating points, by varying the electrical angular speed of the rotor ω_r between 0.2 and 1 pu. For the torque and flux controller, we set the torque weight again to $\lambda_T = 0.052$. The switching penalty is set to $\lambda_{uT} = 0.198 \cdot 10^{-3}$ as in Sect. VI-A. Following

precisely the design guideline (31), the switching penalty of the predictive current controller is set to $\lambda_{uI} = 3.218 \cdot 10^{-3}$.

Fig. 11 shows the current TDD and switching frequency for both control methods when the torque reference is zero. The current TDD is bounded between 6% and 7.5%; it is thus more or less constant across the different speed operating points. The switching frequency, however, varies between 180 and almost 300 Hz. To achieve certain distortions with a three-level converter, a higher switching frequency is required around 25% and 75% of the output voltage than around 50% and 90%. This characteristic is reflected in Fig. 11(b).

Of particular importance is the product $I_{\text{TDD}} \cdot f_{\text{sw}}$ between the current distortions and the switching frequency. This metric characterizes a given modulation method [21]. At a given speed (and thus modulation index), both control methods yield effectively the same performance metric when operating at zero torque, see Fig. 11(c).

(a) Current TDD I_{TDD} (%)   (b) Switching frequency f_{sw} (Hz)   (c) Performance metric $I_{\text{TDD}} \cdot f_{\text{sw}} \cdot 10^{-3}$
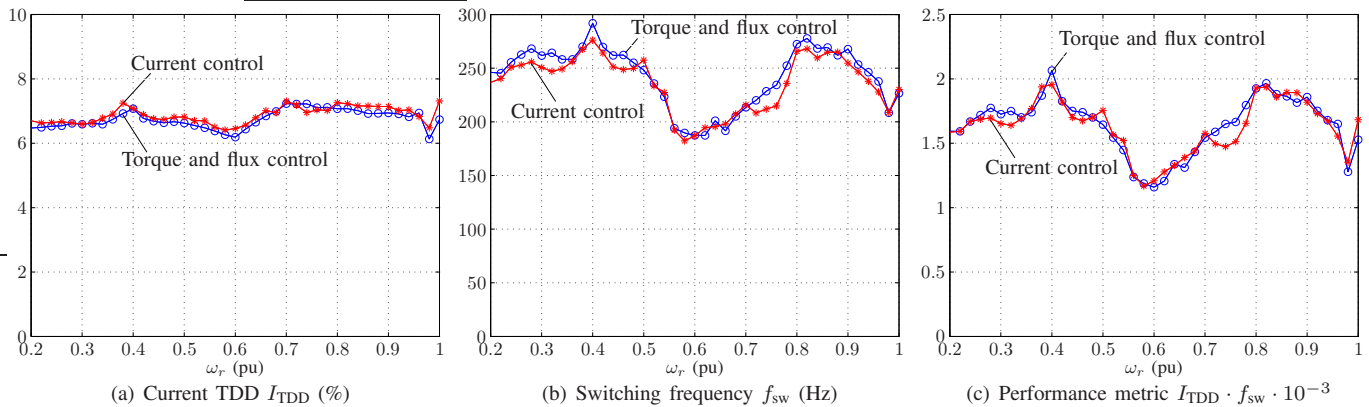
Fig. 11: Predictive torque and flux control versus predictive current control. Operation at zero torque ($T_e^* = 0$ pu) and multiple speed operating points ω_r

(a) Current TDD I_{TDD} (%)   (b) Switching frequency f_{sw} (Hz)   (c) Performance metric $I_{\text{TDD}} \cdot f_{\text{sw}} \cdot 10^{-3}$
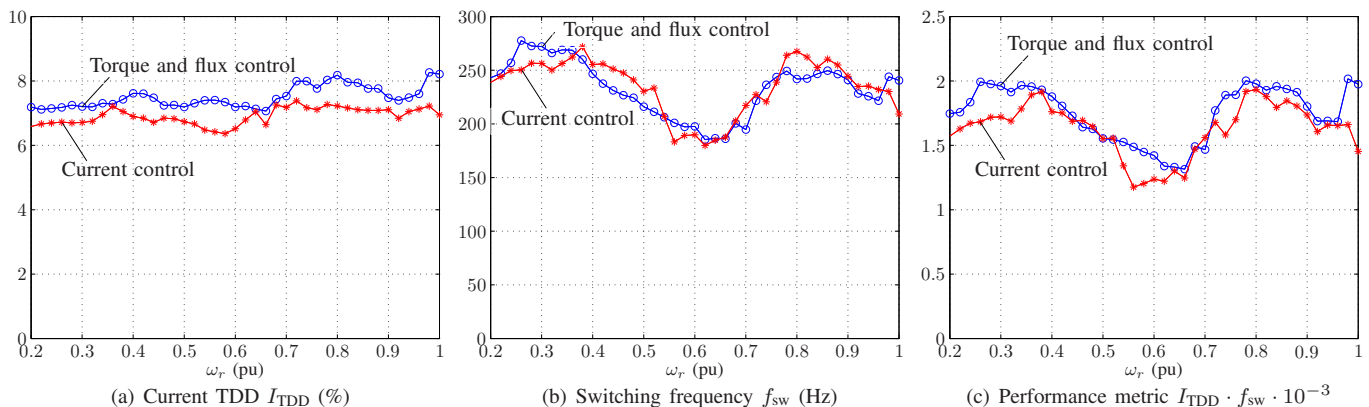
Fig. 12: Predictive torque and flux control versus predictive current control. Operation at rated torque ($T_e^* = 1$ pu) and multiple speed operating points ω_r

At rated torque, the current controller achieves lower current distortions, but tends to require higher switching frequencies to do so, see Figs. 12(a) and 12(b). The performance metric in Fig. 12(c) indicates that, on average, the current controller achieves lower current distortions for a given switching frequency than the torque and flux controller. This observation is in line with the analysis done in Sect. V and the performance analysis in this section.

VII. CONCLUSIONS

We conclude that, in general, the predictive torque and flux controller and the current controller yield similar performance metrics at steady-state operation, provided that the weights are chosen in accordance with the two algebraic design guidelines stated in this paper. The first guideline (28) ensures that the torque and flux controller achieves minimum current distortions per switching frequency. The second guideline (31) ensures a strong performance similarity between the two control schemes. This implies that both controllers achieve similar current and torque distortions and operate at a similar switching frequency. Furthermore, their transient responses in the presence of torque steps are nearly identical.

In light of this similarity, additional criteria could be considered when deciding between the predictive current controller

and the predictive torque and flux controller. Besides the harmonic performance, relevant criteria include the robustness to parameter variations, the simplicity of the outer control loops and the ease with which current constraints could be added.

APPENDIX A: PENALTY ON THE STATOR CURRENT ERROR

The predictive current controller in Sect. IV penalizes the predicted stator current error at time step $k + 1$ in its cost function. The corresponding term J_I, which is defined in (20a), is derived in this appendix.

Assume steady-state operation. In phase a we define the stator current error

$$i_{\text{err},a}(\ell) = i_{sa}^*(\ell) - i_{sa}(\ell) \tag{32}$$

as the difference between the (sinusoidal) stator current reference i_{sa}^* and the stator current i_{sa}. In here, $\ell \in \mathbb{N}$ denotes the discrete time step. The current errors in phases b and c are defined accordingly.

In the time domain, the stator current TDD of phase a is proportional to the root mean square (rms) value of the stator current error $i_{\text{err},a}$ over an infinitely long window. We center

this window at the current time step k and define

$$I_{a,\text{TDD}} = \lim_{\substack{N_1 \to \infty \\ N_2 \to \infty}} \frac{1}{I_{s,\text{nom}}} \sqrt{\frac{1}{N_1 + N_2} \sum_{\ell = k - N_1 + 1}^{k + N_2} i_{\text{err},a}^2(\ell)}, \quad (33)$$

where $I_{s,\text{nom}}$ is the nominal rms stator current. The phase b and c current TDDs are defined accordingly.

The TDD of the three-phase stator current

$$I_{\text{TDD}} = \sqrt{\frac{1}{3}\left(I_{a,\text{TDD}}^2 + I_{b,\text{TDD}}^2 + I_{c,\text{TDD}}^2\right)} \quad (34)$$

is the rms value of the single-phase TDDs.

In an effort to account for the current TDD in the cost function, we interpret N_2 in (33) as the prediction horizon. For the predictive current controller, we set $N_2 = 1$, which approximates (33) as

$$I_{a,\text{TDD}} \approx \lim_{N_1 \to \infty} \frac{1}{I_{s,\text{nom}}} \sqrt{\frac{1}{N_1 + 1} \sum_{\ell = k - N_1 + 1}^{k+1} i_{\text{err},a}^2(\ell)}. \quad (35)$$

By inserting (35) in (34), we obtain the approximation of the squared current TDD

$$\begin{aligned} I_{\text{TDD}}^2 \approx \frac{1}{3 I_{s,\text{nom}}^2} \lim_{N_1 \to \infty} \frac{1}{N_1 + 1} \\ \sum_{\ell = k - N_1 + 1}^{k+1} \left(i_{\text{err},a}^2(\ell) + i_{\text{err},b}^2(\ell) + i_{\text{err},c}^2(\ell)\right). \end{aligned} \quad (36)$$

The sum from $k - N_1 + 1$ to k captures the past current distortions, whereas the time step $k + 1$ corresponds to future current distortions. Only the latter can be influenced by the controller. We thus define the cost function term

$$\begin{aligned} J_I &= \frac{2}{3}\left(i_{\text{err},a}^2(k+1) + i_{\text{err},b}^2(k+1) + i_{\text{err},c}^2(k+1)\right) \\ &= \frac{2}{3}\left(\boldsymbol{i}_{\text{err},abc}(k+1)\right)^T \boldsymbol{i}_{\text{err},abc}(k+1) \end{aligned} \quad (37)$$

with the (seemingly arbitrary) scaling factor $2/3$ and the three-phase stator current error $\boldsymbol{i}_{\text{err},abc} = [i_{\text{err},a} \; i_{\text{err},b} \; i_{\text{err},c}]^T$.

We also define the stator current error in the stationary orthogonal coordinate system as

$$\boldsymbol{i}_{\text{err},\alpha\beta} = \boldsymbol{i}_{s,\alpha\beta}^* - \boldsymbol{i}_{s,\alpha\beta}. \quad (38)$$

Inserting $\boldsymbol{i}_{\text{err},abc} = \boldsymbol{K}^{-1}(0)\boldsymbol{i}_{\text{err},\alpha\beta}$ in (37) and noting that $\boldsymbol{K}^{-T}(0)\,\boldsymbol{K}^{-1}(0) = 1.5\,\text{diag}(1,\,1)$ results in

$$J_I = \left(\boldsymbol{i}_{\text{err},\alpha\beta}(k+1)\right)^T \boldsymbol{i}_{\text{err},\alpha\beta}(k+1) = ||\boldsymbol{i}_{\text{err},\alpha\beta}(k+1)||_2^2. \quad (39)$$

This directly leads to the commonly used cost function term

$$J_I = ||\boldsymbol{i}_{s,\alpha\beta}^*(k+1) - \boldsymbol{i}_{s,\alpha\beta}(k+1)||_2^2 \quad (40)$$

for the stator current error.

Appendix B: Current and Torque TDDs

Low current TDDs imply low torque TDDs, but the converse statement does not necessarily hold true. To show this, we consider in this appendix the current and torque ripples (or steady-state tracking errors), which directly correspond to their respective TDDs.

Recall the torque equation (4) in terms of the rotor flux linkage and the stator current and define the torque reference $T_e^* = \frac{1}{\text{pf}} \frac{X_m}{X_r} \boldsymbol{\psi}_{r,\alpha\beta} \times \boldsymbol{i}_{s,\alpha\beta}^*$. The torque ripple is then given by

$$\begin{aligned} T_{\text{err}} = T_e^* - T_e &= \frac{1}{\text{pf}} \frac{X_m}{X_r} \boldsymbol{\psi}_{r,\alpha\beta} \times \boldsymbol{i}_{\text{err},\alpha\beta} \\ &= \frac{1}{\text{pf}} \frac{X_m}{X_r} \left(\psi_{r\alpha} i_{\text{err},\beta} - \psi_{r\beta} i_{\text{err},\alpha}\right), \end{aligned} \quad (41)$$

where the stator current ripple (or error) was defined in (38). It follows directly from (41) that by minimizing the current ripple in the α- and β-axis, the torque ripple is also minimized. In particular, zero current ripple implies zero torque ripple.

In order to minimize the torque ripple, however, the right-hand side of (41) must be minimized. Zero torque ripple is achieved when the α- and β-components of the current ripple have the same ratio as the α- and β-components of the rotor flux vector, i.e.

$$\frac{i_{\text{err},\alpha}}{i_{\text{err},\beta}} = \frac{\psi_{r\alpha}}{\psi_{r\beta}}. \quad (42)$$

(We neglect here the special case when any of the β-components is zero.) This implies that in order to minimize the torque ripple, the stator current ripple vector must rotate synchronously with the rotor flux vector, but the magnitude of the current ripple vector is not required to be small. In contrast, in order to minimize the current distortions, the current ripple components should be of the same magnitude and as small as possible, as discussed in Appendix A.

When increasing for the predictive torque and flux controller the weight λ_T in the cost function (10) beyond the value that provides close-to-circular bounds, the torque ripple is penalized strongly, whereas the stator flux magnitude ripple is penalized less. Owing to (23), with $X_r/D = 3.92$ in our particular case, the current ripple is penalized significantly less. Large λ_T thus reduce the torque ripple but tend to increase the current ripple. We conclude that very low torque distortions can be achieved with predictive torque and flux control, albeit at the expense of pronounced current distortions.

References

[1] P. Cortés, M. P. Kazmierkowski, R. M. Kennel, D. E. Quevedo, and J. Rodríguez, "Predictive control in power electronics and drives," *IEEE Trans. Ind. Electron.*, vol. 55, pp. 4312–4324, Dec. 2008.

[2] S. Kouro, P. Cortés, R. Vargas, U. Ammann, and J. Rodríguez, "Model predictive control—A simple and powerful method to control power converters," *IEEE Trans. Ind. Electron.*, vol. 56, pp. 1826–1838, Jun. 2009.

[3] J. Rodríguez, M. P. Kazmierkowski, J. R. Espinoza, P. Zanchetta, H. Abu-Rub, H. A. Young, and C. A. Rojas, "State of the art of finite control set model predictive control in power electronics," *IEEE Trans. Ind. Informatics*, vol. 9, pp. 1003–1016, May 2013.

[4] J. Rodríguez, J. Pontt, C. Silva, P. Cortés, U. Ammann, and S. Rees, "Predictive direct torque control of an induction machine," in *Proc. IEEE Power Electron. and Motion Control Conf.*, (Riga, Latvia), 2004.

[5] H. Miranda, P. Cortés, J. I. Yuz, and J. Rodríguez, "Predictive torque control of induction machines based on state-space models," *IEEE Trans. Ind. Electron.*, vol. 56, pp. 1916–1924, Jun. 2009.

[6] P. Cortés, S. Kouro, B. L. Rocca, R. Vargas, J. Rodríguez, J. I. León, S. Vazquez, and L. G. Franquelo, "Guidelines for weighting factors design in model predictive control of power converters and drives," in *Proc. IEEE Int. Conf. Ind. Technol.*, 2009.

[7] S. Thielemans, T. Vyncke, and J. Melkebeek, "Weight factor selection for model-based predictive control of a four-level flying-capacitor inverter," *IET Power Electron.*, vol. 5, pp. 323–333, Mar. 2012.

[8] R. Vargas, U. Ammann, B. Hudoffsky, J. Rodriguez, and P. Wheeler, "Predictive torque control of an induction machine fed by a matrix converter with reactive input power control," *IEEE Trans. Power Electron.*, vol. 25, pp. 1426–1438, Jun. 2010.

[9] J. Rodriguez, R. M. Kennel, J. R. Espinoza, M. Trincado, C. A. Silva, and C. A. Rojas, "High-performance control strategies for electrical drives: An experimental assessment," *IEEE Trans. Ind. Electron.*, vol. 49, pp. 812–820, Feb. 2012.

[10] P. Zanchetta, "Heuristic multi-objective optimization for cost function weights selection in finite states model predictive control," in *Workshop on Pred. Control of Electr. Drives and Power Electron.*, (Munich, Germany), Oct. 2011.

[11] S. A. Davari, D. A. Khaburi, and R. Kennel, "An improved FCS-MPC algorithm for an induction motor with an imposed optimized weighting factor," *IEEE Trans. Power Electron.*, vol. 27, pp. 1540–1551, Mar. 2012.

[12] C. Rojas, J. Rodríguez, F. Villarroel, J. Espinoza, C. Silva, and M. Trincado, "Predictive torque and flux control without weighting factors," *IEEE Trans. Ind. Electron.*, vol. 60, pp. 681–690, Feb. 2013.

[13] K. Hasse, "Zum dynamischen Verhalten der Asynchronmaschine bei Betrieb mit variabler Ständerfrequenz und Ständerspannung," *ETZ-A*, vol. 89, pp. 387–391, 1968.

[14] T. Laczynski and A. Mertens, "Predictive stator current control for medium voltage drives with *LC* filters," *IEEE Trans. Power Electron.*, vol. 24, pp. 2427–2435, Nov. 2009.

[15] S. Müller, U. Ammann, and S. Rees, "New modulation strategy for a matrix converter with a very small mains filter," in *Proc. IEEE Power Electron. Spec. Conf.*, (Acapulco, Mexico), Jun. 2003.

[16] J. Rodríguez, J. Pontt, C. Silva, M. Salgado, S. Rees, U. Ammann, P. Lezana, R. Huerta, and P. Cortés, "Predictive control of three-phase inverter," *IET Electronics Letters*, vol. 40, pp. 561–563, Apr. 2004.

[17] J. Rodríguez, J. Pontt, C. A. Silva, P. Correa, P. Lezana, P. Cortés, and U. Ammann, "Predictive current control of a voltage source inverter," *IEEE Trans. Ind. Electron.*, vol. 54, pp. 495–503, Feb. 2007.

[18] R. Vargas, P. Cortés, U. Ammann, J. Rodríguez, and J. Pontt, "Predictive control of a three-phase neutral-point-clamped inverter," *IEEE Trans. Ind. Electron.*, vol. 54, pp. 2697–2705, Oct. 2007.

[19] J. Holtz, "Pulsewidth modulation—A survey," *IEEE Trans. Ind. Electron.*, vol. 32, pp. 410–420, Dec. 1992.

[20] T. Geyer, "Model predictive direct current control: Formulation of the stator current bounds and the concept of the switching horizon," *IEEE Ind. Appl. Mag.*, vol. 18, pp. 47–59, Mar./Apr. 2012.

[21] T. Geyer, "A comparison of control and modulation schemes for medium-voltage drives: Emerging predictive control concepts versus PWM-based schemes," *IEEE Trans. Ind. Appl.*, vol. 47, pp. 1380–1389, May/Jun. 2011.

[22] T. Geyer, "Algebraic weighting factor selection for predictive torque and flux control," in *Proc. IEEE Energy Convers. Congr. Expo.*, (Cincinnati, OH, USA), Oct. 2017.

[23] T. Geyer and D. E. Quevedo, "Multistep finite control set model predictive control for power electronics," *IEEE Trans. Power Electron.*, vol. 29, pp. 6836–6846, Dec. 2014.

[24] T. Geyer and D. E. Quevedo, "Performance of multistep finite control set model predictive control for power performance," *IEEE Trans. Power Electron.*, vol. 30, pp. 1633–1644, Mar. 2015.

[25] P. C. Krause, O. Wasynczuk, and S. D. Sudhoff, *Analysis of electric machinery and drive systems*. Wiley, 2nd ed., 2002.

[26] T. Geyer, *Model predictive control of high power converters and industrial drives*. London, UK: Wiley, Oct. 2016.